

Article

Mesoscopic Mapping of Visual Pathway in a Female 5XFAD Mouse Model of Alzheimer's Disease

Yunkwon Nam ^{1,†}, Sujin Kim ^{1,2,†}, Jieun Kim ^{3,†}, Hyang-Sook Hoe ^{3,4,*} and Minhoo Moon ^{1,2,*}¹ Department of Biochemistry, College of Medicine, Konyang University, Daejeon 35365, Republic of Korea² Research Institute for Dementia Science, Konyang University, Daejeon 35365, Republic of Korea³ Department of Neural Development and Disease, Korea Brain Research Institute (KBRI), Daegu 41068, Republic of Korea⁴ Department of Brain & Cognitive Sciences, Daegu Gyeongbuk Institute of Science & Technology (DGIST), Daegu 42988, Republic of Korea

* Correspondence: sookhoe72@kbri.re.kr (H.-S.H.); hominmoon@konyang.ac.kr (M.M.)

† These authors contributed equally to this work.

Abstract: Amyloid- β ($A\beta$) deposition and $A\beta$ -induced neurodegeneration appear in the retina and retinorecipient areas in the early stages of Alzheimer's disease (AD). Although these $A\beta$ -related changes in the retina cause damage to the visual functions, no studies have yet revealed the alterations in the visual pathways of AD. Therefore, we investigated the alterations of visual circuits in the AD mouse model using anterograde tracer cholera toxin β subunits (CT β). Moreover, we investigated the $A\beta$ accumulation in the retina and retinorecipient areas and the neuronal loss, and synaptic degeneration in retinorecipient areas by immunofluorescent staining of 4- and 12-month-old female 5XFAD transgenic mice. Our results demonstrated that $A\beta$ accumulation and neurodegeneration occurred in the retina and retinorecipient regions of early and late stages of the 5XFAD mice. Retinal efferents to the suprachiasmatic nucleus and lateral geniculate nucleus were impaired in the early stage of AD. Moreover, retinal connections to the dorsal lateral geniculate nucleus and superior colliculus were degenerated in the late-stage of AD. These findings reveal the $A\beta$ -related pathology induced visual circuit disturbances at the mesoscale level in both the early and late stages of AD and provide anatomical and functional insights into the visual circuitry of AD.

Keywords: Alzheimer's disease; visual pathway; 5XFAD mice; cholera toxin β subunits

Citation: Nam, Y.; Kim, S.; Kim, J.; Hoe, H.-S.; Moon, M. Mesoscopic Mapping of Visual Pathway in a Female 5XFAD Mouse Model of Alzheimer's Disease. *Cells* **2022**, *11*, 3901. <https://doi.org/10.3390/cells11233901>

Academic Editors: Cristine Alves Da Costa and Daniele Nosi

Received: 22 September 2022

Accepted: 1 December 2022

Published: 2 December 2022

Publisher's Note: MDPI stays neutral with regard to jurisdictional claims in published maps and institutional affiliations.



Copyright: © 2022 by the authors. Licensee MDPI, Basel, Switzerland. This article is an open access article distributed under the terms and conditions of the Creative Commons Attribution (CC BY) license (<https://creativecommons.org/licenses/by/4.0/>).

1. Introduction

Amyloid- β ($A\beta$) peptides, one of the causative factors in Alzheimer's disease (AD), are natural products of metabolism consisting of 36–43 amino acids. Under pathological conditions, the production functions of $A\beta$ increase, and the clearance functions decrease. An imbalance between the production and elimination functions of these $A\beta$ increases the aggregation and accumulation of $A\beta$ [1]. Notably, the intermediate and soluble oligomer $A\beta$ forms provoke neurodegeneration including neuronal death and synaptic loss in the brain [2]. Interestingly, a study in which $A\beta$ was injected into neurons using a patch pipette reported that intracellular accumulation of $A\beta$ induces synaptic dysfunction [3]. The neurotoxic and synaptotoxic $A\beta$ directly attenuates the neural circuit networks in the brains affected by AD [4–7]. A decrease in structural and functional connectivity of neural circuit networks directly affects the onset and progression of AD symptoms [8,9]. Impairments in various neural circuits and brain networks that underlie cognitive, behavioral, and sensory systems could result in cognitive decline, emotional deficit, and sensory loss in AD [10]. Consequently, circuit disturbances and network disruptions resulting from $A\beta$ toxicity directly induce the accompanying dysfunctions of various systems in AD. Therefore, it is essential to know which circuits and networks are altered and damaged in AD.

Visual impairments, such as low visual acuity and reduced contrast sensitivity, are common in patients with AD [11]. Many studies have reported that retinal ganglion cells (RGCs), particularly intrinsically proprioceptive retinal ganglion cells (ipRGCs), and the retinal nerve fiber layer (RNFL) are severely damaged in AD [12–14]. These RGCs and RNFL undergo extensive damage in the early stage of AD without visual failure [13,15]. It suggests that pathophysiologic alterations have already appeared in the eyes of the early stage of AD. Indeed, A β accumulation and neuronal loss were significantly increased in the retina of AD patients compared to healthy controls [16]. Similar to the results of the AD patients, A β accumulation in the retina precedes A β deposition in AD mouse models [17,18]. Moreover, damaged inner retina induced by A β aggregation precedes neuronal cell death in other brain regions [18]. Taken together, A β -induced deficiency of RGCs and RNFLs appears from the early stages of AD, and this deficiency can lead to impaired connectivity between the retina and retinorecipient areas. Therefore, alterations in the visual pathway from the eye to the brain could affect visual dysfunction in AD.

In the brain, retinorecipient areas originating from the eye include 25 ipsilateral brain regions and 34 contralateral brain regions [19]. The major retinorecipient areas are the lateral geniculate nucleus (LGN), superior colliculus (SC), suprachiasmatic nucleus (SCN), olivary pretectal nucleus (OPN), and medial terminal nucleus (MTN) of the accessory optic tract [20]. The LGN is divided into subregions, such as the dorsal lateral geniculate nucleus (dLGN), intergeniculate leaflet (IGL), and ventral lateral geniculate nucleus (vLGN) [21]. Although the connectivity between retina and retinorecipient regions in the healthy brain is well known, no studies the alterations of the visual pathways in the brains with AD. Moreover, it has been shown that A β -induced deficiency of RGC and RNFL appears in the early stages of AD, resulting in visual pathway impairment. Therefore, a hypothesis was formulated stating that the visual pathway could be altered in A β -overexpressing transgenic mice before cognitive decline as the primary symptom of AD. Importantly, visual behavioral deficits in AD patients are known to occur at the prodromal stage of AD [10]. Likewise, it has been reported that visual-related behavioral deficits, such as circadian rhythm (sleep-wake) disturbance and visual acuity (optokinetic system) impairment, appear in 5XFAD mice between 4 and 6 months of age [22,23]. Herein, we focused on the topographical changes in visual pathways before and after cognitive impairment. We selected 4-month-old 5XFAD mice corresponding to prodromal stage of AD [24] and 12-month-old 5XFAD mice corresponding to severe stage of AD [25]. To reveal the connections from the retina to retinorecipient areas in AD, we used the cholera toxin β subunit (CT β) conjugated to Alexa-Fluor 488 as a tracer. CT β is a non-transsynaptic neural tracer widely used for monosynaptic mapping since it lacks transsynaptic tracing [26]. In addition, CT β is a reliable tracer widely used to evaluate the anterograde transport of RGCs [17,27,28].

2. Materials and Methods

2.1. Animals

The five familial AD mutations (5XFAD) mice express three mutations in the human *APP* gene (Florida I716V, Swedish K670N/M671L, and London V717I) and two mutations in the human *PSEN1* gene (L286V and M146L). The animals were purchased from the Jackson Laboratory in Bar Harbor, Mainer, ME, USA (#006554). The present study used 4- and 12-month-old female 5XFAD mice and wild-type (WT) littermates. The 5XFAD mice are A β -overexpressing transgenic mice with five familial AD mutations, generally showing significant cognitive impairment from 6 months of age and neurodegeneration from 9 months of age [29,30]. As previously described [31], the 5XFAD transgenic mice were identified through genotyping of tail DNA. Moreover, some 5XFAD and WT littermate mice start to exhibit retinal degeneration and lose sight at 35 days of age as a result of phosphodiesterase-6b retinal degeneration-1 (*Pde6b^{rd1}*) allele in the SJL/J background strain [32]. *Pde6b^{rd1}* has an autosomal recessive inheritance pattern [33]. Thus, mice with retinal degeneration *Pde6b^{rd1}* mutation were classified and excluded using genotyping (Mutant: 5-AAG CTA GCT GCA GTA ACG CCA TTT-3, Wild-type: 5-ACC TGC ATG TGA

ACC CAG TAT TCT ATC-3, Common: 5-CTA CAG CCC CTC TCC AAG GTT TAT AG-3). WT and 5XFAD mice excluding *Pde6b^{rd1}* mutants were randomly assigned into four groups: (1) 4-month-old WT mice (n = 5), (2) 4-month-old 5XFAD mice (n = 5), (3) 12-month-old WT mice (n = 5), and (4) 12-month-old 5XFAD mice (n = 5). Maintenance and treatment of the animals were performed as per the principles of the Care and Use of Laboratory Animals (NIH Publication No. 85-23, revised 1985) and the Animal Care and Use Guidelines of Konyang University (Project code: P-18-06-A-01). Every attempt was made to keep the animals alive and their suffering to a minimum.

2.2. Intravitreal Injections

In a mouse, 85–90% of optic nerve axons decussate to the other side of the brain [34]. In addition, it has been reported that axons arising from the nasal retina project through the contralateral optic tract to the contralateral brain [35]. Thus, we injected CT β intravitreally towards the nasal retina. All the animals were anesthetized with a dose of 250 μ g/kg Avertin (Tribromoethanol; Sigma-Aldrich, St. Louis, MO, USA). The intravitreal injection was performed using a microscope (Leica, stereozoom S9 D). A sharp 30-gauge needle was inserted into the edge of the right eye to make a small incision and 1 μ L of vitreous fluid was subsequently withdrawn using a blunt 33-gauge needle attached to a Hamilton syringe. Finally, 1 μ L of 1 mg/mL CT β conjugated to Alexa-Fluor 488 (Thermo Fisher Scientific Inc., Waltham, MA, USA) was injected into the right eye using the same Hamilton syringe [17]. In order to prevent eye damage, a needle was placed between the lens and the retina, and eye ointment was applied following the intravitreal injection.

2.3. Brain Tissue and Retina Wholemout Preparation

We analyzed the mouse's left brain, contralateral to the right eye. The animals were anesthetized for three days following the CT β injections, transcardially perfused with 0.05 M phosphate-buffered saline (PBS), and subsequently fixed with cold 4% paraformaldehyde in 0.1 M phosphate buffer (PB). Thereafter, the eyes and brain tissues were extracted, and the tissues were post-fixed in 0.1 M PB containing 4% paraformaldehyde for 20 h at 4 °C. For cryoprotection, the brains were subsequently immersed in 30% sucrose in 0.05 M PBS solution for 3 days at 4 °C. The brains were subsequently embedded in Surgipath[®] frozen section compound (Leica Biosystems, Wetzlar, Germany) and sliced into serial 30- μ m-thick coronal slices using a CM1850 cryostat (Leica Biosystems). As previously described [36], for the retina wholemount preparation, the eye tissues were dissected to remove the lens, vitreous, and retinal pigment epithelium, and the retina was collected. Then, quadrants of the retina were cut and spread flat on the glass.

2.4. Immunofluorescence Labeling

To investigate the immunoreactivity of A β accumulation, the retina and brain tissues were incubated using a blocking solution (0.05% bovine serum albumin, 1.5% normal goat serum, and 0.3% Triton X-100 in PBS) and mouse anti-4G8 antibody specific for A β ₁₇₋₂₄ (1:2000; BioLegend, San Diego, CA, USA) overnight at 4 °C. To examine the immunoreactivity of neuronal nuclei (NeuN) and synaptophysin (SYN), free-floating brain sections were incubated overnight at 4 °C with the mouse anti-NeuN antibody (1:1000; Cat.# MAB377, Merk KGaA, Darmstadt, Germany) or mouse anti-SYN antibody (1:500; Cat.#S5768, Sigma-Aldrich), respectively, in blocking solution. Additionally, the retina and brain tissues were incubated with donkey Alexa 488-conjugated anti-mouse IgG (1:200; Thermo Fisher Scientific Inc., Waltham, MA, USA) or donkey Alexa 594-conjugated anti-mouse IgG (1:200; Thermo Fisher Scientific Inc.) for 1 h at room temperature. To counterstain the nuclei, the retina and brain tissues were mounted on ProbeOnTM Plus Microscope Slides (Thermo Fisher Scientific Inc.) and covered with FluoroshieldTM with 4',6-diamidino-2-phenylindole (DAPI) (Sigma-Aldrich).

2.5. Image Acquisition and Analysis

All the brain and retinal tissues labeled with CT β and 4G8, NeuN, and SYN staining were imaged using a Zeiss LSM 700 Meta confocal microscope (Carl Zeiss AG, Oberkochen, Germany) and analyzed using ImageJ software (National Institutes of Health, Bethesda, MD, USA). To quantify the percentage of 4G8 (+) area 20 to 40 images of the immunostained retina sections were quantified as follows (Supplementary Figures S1 and S2); (1) the images were changed to 8-bit images; (2) the images were thresholded to eliminate background signals; (3) sorting the 4G8 (+) labeled signals (>20 μm); (4) the thresholded images of the defined retina region were quantified by the “analyze particles” tool for the “% area” measurement of the 4G8 (+) labeled signals. To quantify the number NeuN (+) cells per mm^2 , 20 to 40 images of the immunostained brain sections were quantified as follows: (1) the positively-stained areas (10–20 μm) were manually outlined using the paintbrush tool; (2) the images were changed to 8-bit images; (3) the images were thresholded to eliminate background signals; (4) the anatomical retinorecipient regions of the SC, LGN, IGL, and SCN were defined based on DAPI; (5) the thresholded images of the defined brain region were quantified using the “analyze particles” tool and the “count” value was read; and (6) the “count” value was divided by the area of the defined region. Last, the methods of measurement of the optical density of SYN immunoreactivity and CT β -labeled axon terminal were as follows: (1) manually removing excessively merged forms around the A β plaque; (2) manually drawing the region of interest (ROI); (3) selecting “analyze” and “measure” to give a numerical measurement to the fluorescence of the ROI. In particular, values of the CT β -labeled axon terminal from the four groups were normalized to the controls using the following equations: % of control = (fluorescence intensity of WT or 5XFAD mice/fluorescence intensity average of WT mice) \times 100.

2.6. Statistical Analysis

All the data were analyzed by GraphPad Prism 7 (Systat Software, La Jolla, CA, USA). Analyzed values are plotted as mean \pm standard error of the mean (SEM). Data were analyzed using independent t-tests between the two groups and two-way analysis of variance (ANOVA) was performed between the four groups followed by Tukey’s post hoc tests. A *p*-value of less than 0.05 was considered statistically significant. Image acquisition, quantification, and statistical analysis of each group were blindly performed.

3. Results

3.1. Histological Profiling of the A β Accumulation and Retinal Projections to the Brain

To investigate the retinorecipient areas and retinal pathways in the brain with AD, we injected CT β , a non-transsynaptic anterograde tracer, into the vitreous of WT and 5XFAD mice (Figure 1A). Three days following the intravitreal injection, the fluorescence of CT β conjugated to Alexa-Fluor 488 was detected in the retina (Supplementary Figure S3). Next, we investigated the subcellular localization of CT β in the retinal flat mount using Z-stack imaging. CT β fluorescence signals were localized in the cytoplasm of retinal cells stained with DAPI (Figure 1B–D). This suggests that retinal cells present in the RGCs layer, a layer in which many cells are distributed, endocytosed CT β . Moreover, to examine whether A β accumulations were deposited in the retinal RGCs, we immunofluorescence staining was conducted using anti-4G8 antibody of 4-month- and 12-month-old 5XFAD mice (Figure 1E). We found that A β peptides were significantly aggregated in the retina of 12-month-old 5XFAD compared to 4-month-old 5XFAD mice (Figure 1F). A β accumulates little in the retina of WT mice [22,37] (Supplementary Figure S4). These data suggest that A β accumulation increases with AD progression.

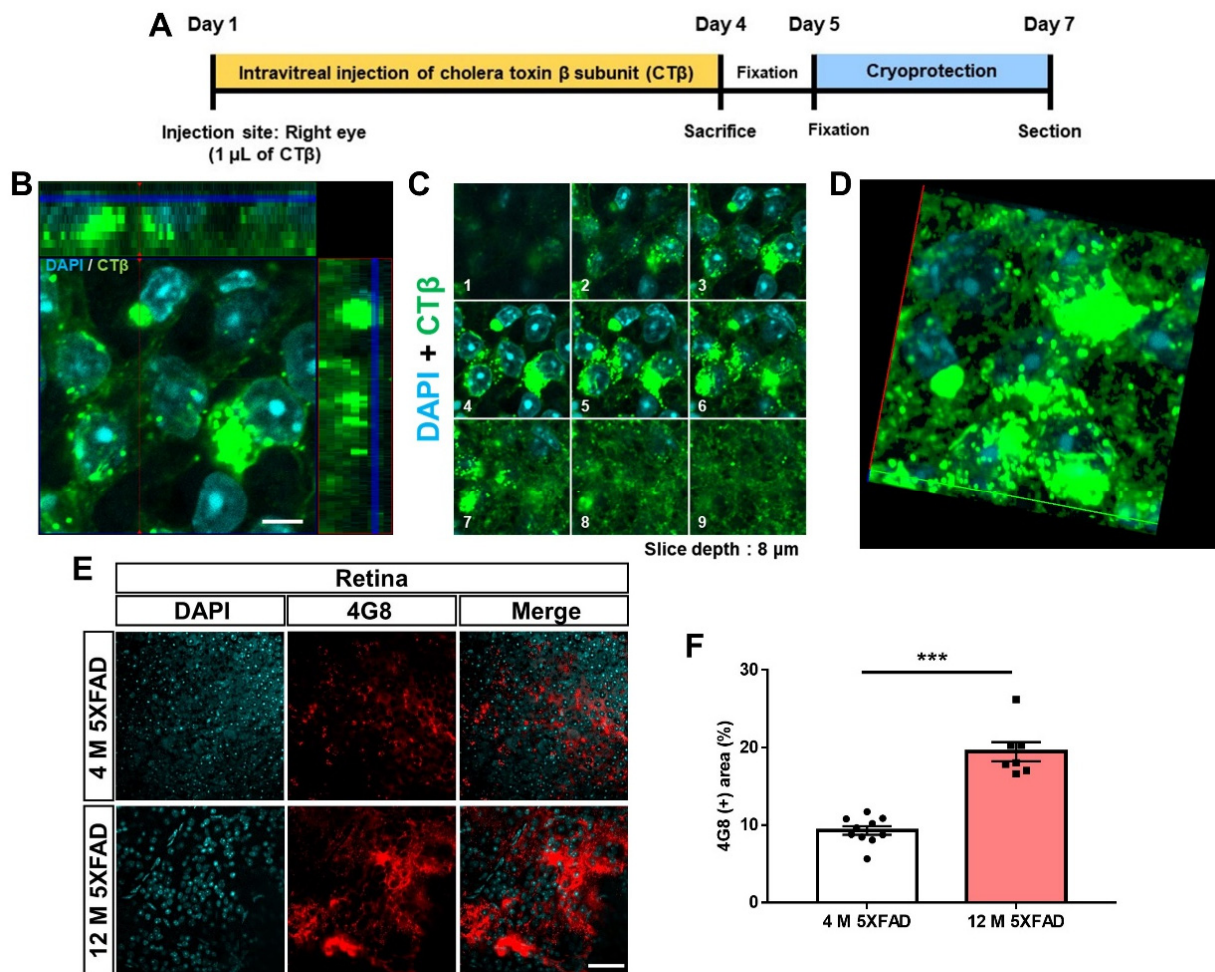


Figure 1. Validation of the application of cholera toxin β subunit (CT β) and characterization of amyloid- β (A β) deposition in the retina. (A) The schematic diagram shows the overall experimental design. (B) An orthogonal view of the z-stack images indicates that the CT β has an intracellular localization in retinal cells. The side and bottom panels, respectively, depict y-z and x-z cross-sectional images. Scale bar = 5 μ m. (C) Serial z-stack images consist of 9 sections at 1- μ m intervals. (D) The representative image shows a three-dimensional z-projection of the acquired stack. (E) The representative image shows A β accumulation in the retina by immunohistochemical staining with anti-4G8 antibody. Scale bar = 50 μ m. (F) The quantitative graph exhibits the area fraction of A β in the retina of 5XFAD mice (7–10 images of the retina wholemount sections were obtained from 5 mice in each group). Statistical analysis was conducted by an independent *t*-test. *** $p < 0.001$ indicate a significant difference.

Subsequently, we compared the retinal efferents to the brain regions of the healthy and AD animals (Figure 2A,B). CT β was mainly co-localized with SYN (Figures 2C and S5). This result suggests that CT β endocytosed into RGCs is transported to their axon terminals reaching the retinorecipient regions. As in previously reported studies [19,20], the signals of CT β axonally transported from retina were detected in retinorecipient areas, including the SCN, OPN, LGN, SC, and MTN of WT and 5XFAD mice (Figure 2D,F,G). Moreover, we characterized A β deposition in retinorecipient areas of 4- and 12-month-old 5XFAD mice (Figure 2E,H,K). A β accumulation was not observed in the SCN, SC, and MTN of 4- and 12-month-old 5XFAD mice (Figure 2E,I,K). Interestingly, A β accumulation was not detected in the OPN of 4-month-old 5XFAD mice, whereas A β deposition was observed in 12-month-old 5XFAD mice (Figure 2H). The LGN showed A β deposition in both 4- and 12-month-old 5XFAD mice (Figure 2J).

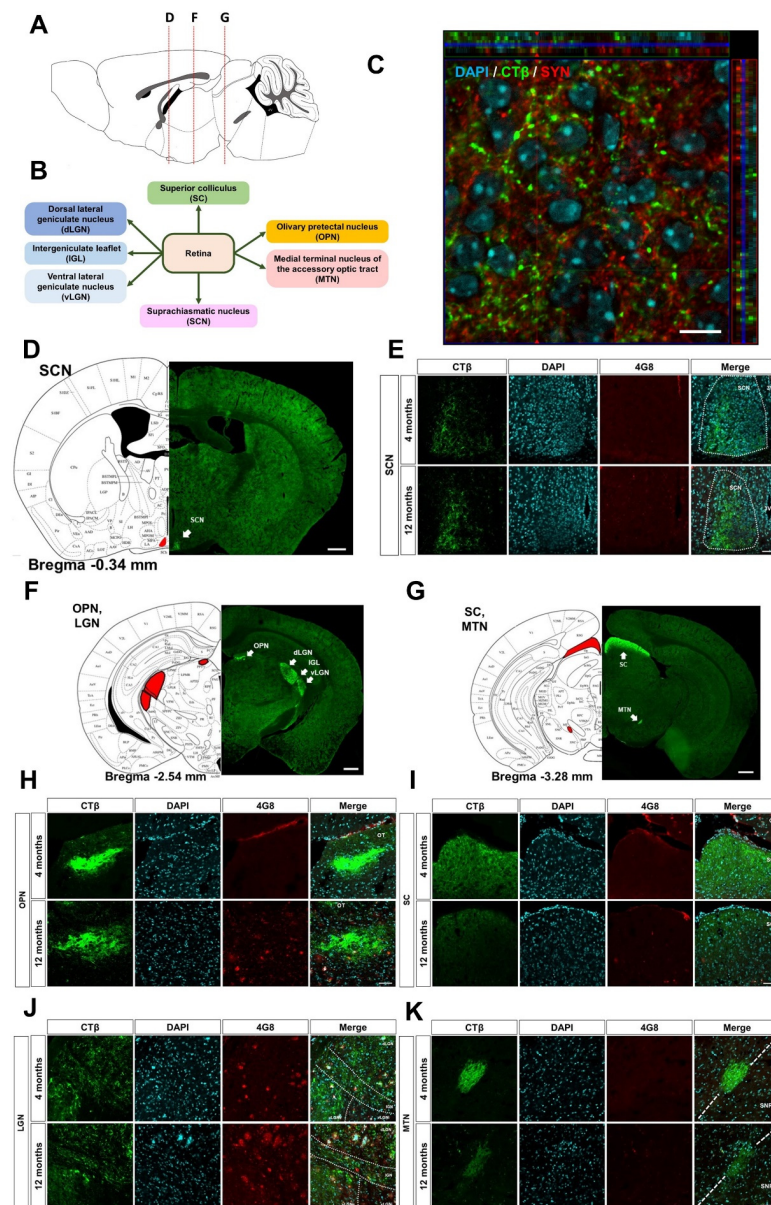


Figure 2. Histological profiling of the CTβ and Aβ deposition in the retinorecipient regions. (A) The sagittal plane of the mouse brain indicates the positions of the representative Figure 2 in (D,F,G). (B) The schematic diagram indicates the projection from the retina to the retinorecipient regions of the brain. CTβ-positive signals represent the retinal output to the (D) SCN, (F) OPN/LGN, and (G) SC/MTN in the brain hemisphere. Scale bar = 500 μm. (C) The representative orthogonal view shows that CTβ co-localizes with the presynaptic vesicular protein synaptophysin (SYN) in the SCN. Green indicated CTβ-positive signals. Red signals showed SYN-positive signals. The side and bottom panels, respectively, depict the y–z and x–z cross-sectional images. Scale bar = 10 μm. Representative images show the deposition of Aβ plaques stained with 4G8 antibody in the (E) SCN, (H) OPN, (I) SC, (J) LGN, and (K) MTN of 4- and 12-month-old 5XFAD groups. Scale bar = 50 μm. The dotted line in (J) indicates the sub-region of the LGN. LGN is divided into dLGN, IGL, external and internal vLGN. (K) MTN is located at the boundary of SNR. dLGN, dorsal lateral geniculate nucleus; IGL, intergeniculate leaflet; LGN, lateral geniculate nucleus; MTN, medial terminal nucleus of the accessory optic tract; OPN, olivary pretectal nucleus; OT, nucleus of the optic tract; SC, superior colliculus; SCN, suprachiasmatic nucleus; SNR, substantia nigra pars reticula; vLGN, ventral lateral geniculate nucleus.

3.2. Disruption of the Retina-SCN Connections in Animal Model of AD

It is well-known that the RGCs project to the SCN of the hypothalamus [38]. In order to visualize the neural connections from the retina to the SCN, we injected CT β into the vitreous of 4- and 12-month-old WT and 5XFAD mice. CT β -positive signals were detected in the SCN of all the mouse groups (Figure 3A,B). To examine whether the retina-SCN pathway is altered in A β -overexpressing brains, we compared the fluorescence signals of CT β in the SCN of the 5XFAD and WT mice. The 5XFAD group showed reduced CT β fluorescence intensity in the SCN compared to the WT group [genotype: $F(1,109) = 47.2$, $p < 0.0001$], and the genotype difference was greater at 4 months than at 12 months. In addition, the fluorescence intensity of CT β decreased with age [age: $F(1,109) = 44.9$, $p < 0.0001$], and the decrease was greater in the WT group than in the 5XFAD group. Moreover, a significant interaction between genotype and age was observed [interaction: $F(1,109) = 23.84$, $p < 0.0001$] (Figure 3C,D). Our findings show that no further impairment of the retina-SCN pathway is seen between 4- and 12-month-old 5XFAD mice since the impairment of the retina-SCN connection is thought to already reach a threshold in 4-month-old 5XFAD mice. Additionally, connectivity from the retina to the SCN is vulnerable to damage by normal aging. Consequently, these results suggest that the efferent projection from the retina to the SCN is seriously impaired before the prodromal stage of AD and is also impaired by the normal aging process.

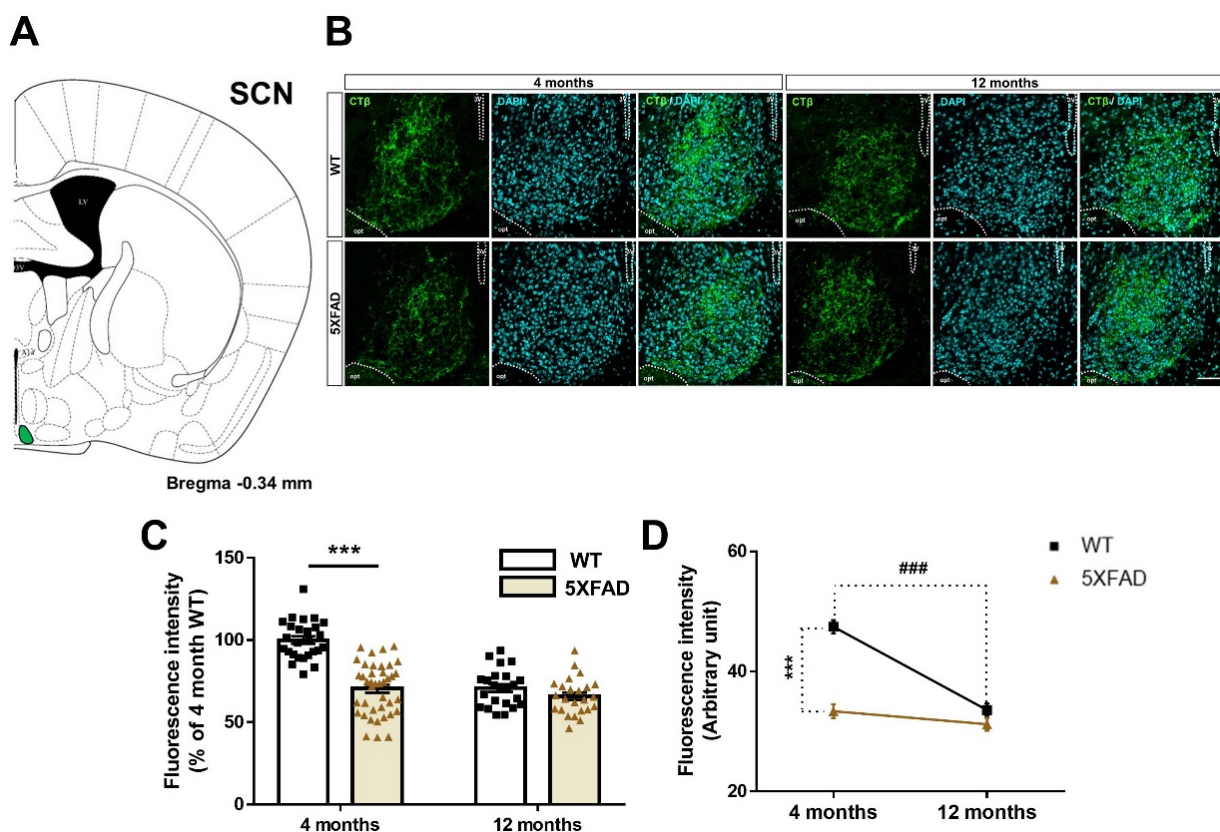


Figure 3. Impairment of the retina-suprachiasmatic nucleus (SCN) pathway in WT and 5XFAD mice. (A) Diagram of a mouse brain section explaining the location of the SCN. (B) The representative image shows CT β -labeled terminal buttons of the axon in the SCN of 4- and 12-month-old WT and 5XFAD mice. Scale bar = 50 μ m. (C) The quantitative graph exhibits the fluorescence intensity of the CT β (+) area in the SCN of WT and 5XFAD mice (24–40 images of the brain sections were obtained from 5 mice in each group). (D) Comparison of the impairment of the retina-SCN pathway by aging and AD progression. Statistical analysis was conducted by two-way ANOVA, followed by Tukey's post hoc test. *** $p < 0.001$ and ### $p < 0.001$ indicate a significant difference.

3.3. Tracing the Retina-OPN Pathways in the 5XFAD Mice

To investigate whether the retinal outputs to OPN are altered in A β -overexpressing brains, we traced the transport of the anterograde tracer from the retina to the OPN in the 4- and 12-month-old WT and 5XFAD mice (Figure 4A,B). There was no difference in the fluorescence intensity of CT β between WT and 5XFAD mice [genotype: $F(1,69) = 0.1837$, $p = 0.6695$]. Similarly, there was no difference of fluorescence intensity of CT β between 4 months and 12 months groups [age: $F(1,69) = 1.019$, $p = 0.3162$]. Moreover, the retina-OPN connectivity did not show genotype \times age interaction [interaction: $F(1,69) = 0.5011$, $p = 0.4814$] (Figure 4C,D). Our findings demonstrate that the retina-OPN pathway is rarely altered by AD progression and normal aging.

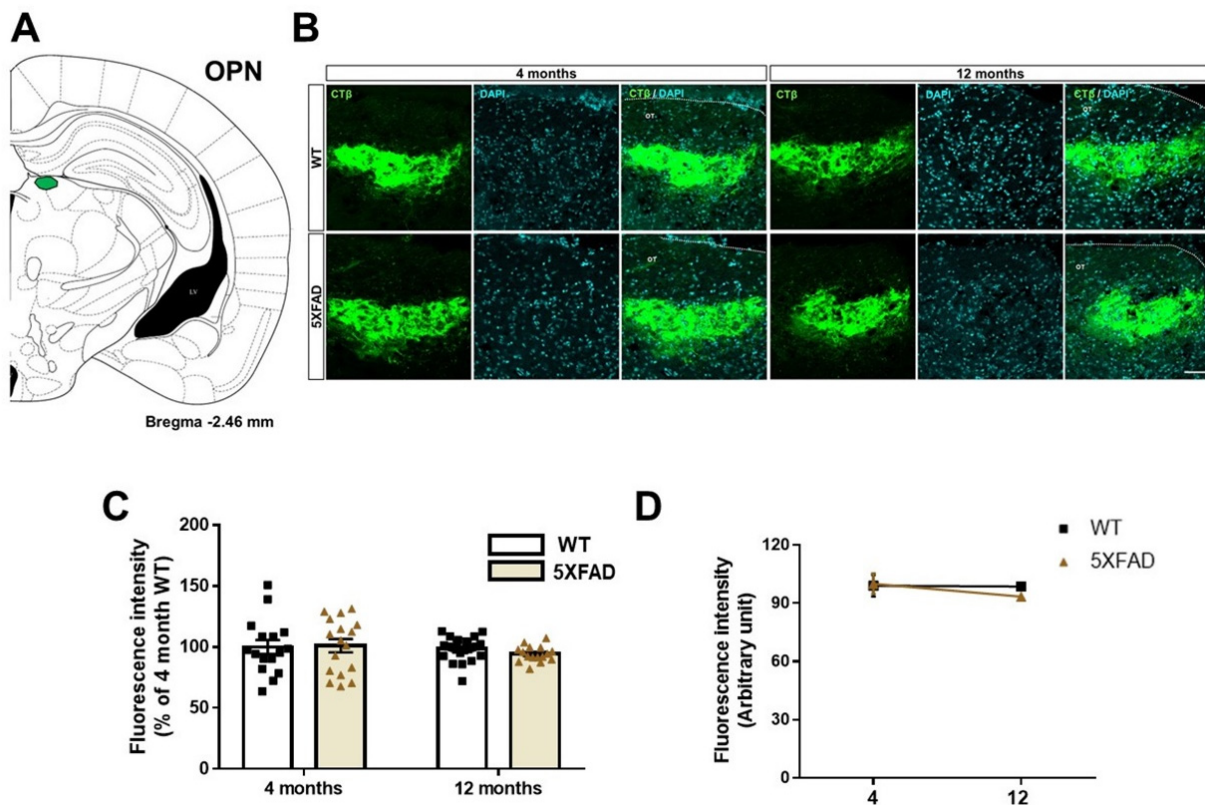


Figure 4. Anatomical tracing of the retina-olivary pretectal nucleus (OPN) pathways in WT and 5XFAD mice. (A) Diagram of a mouse brain section illustrating the location of the OPN. (B) The representative images show CT β transported from the retina to the OPN. Scale bar = 50 μ m. (C) The quantitative graphs exhibit the fluorescence intensity of the CT β (+) areas in the OPN of the WT and 5XFAD mice (16–24 images of the brain sections were obtained from 5 mice in each group). (D) Comparison of the impairment of the retina-OPN projection by aging and AD progression. Statistical analysis was conducted by two-way ANOVA, followed by Tukey’s post hoc test.

3.4. Decreased Retina-LGN Connectivity in the 5XFAD Mice

The LGN is a crucial region in the visual pathway that relays visual information from the retina to the primary visual cortex [39]. We analyzed CT β -positive signals in the three subregions of LGN, such as dLGN, IGL, and vLGN, in 4- and 12-month-old WT and 5XFAD groups (Figure 5A,B). First, the 5XFAD group showed decreased CT β -positive signals compared to the WT group in the dLGN [genotype: $F(1,177) = 62.58$, $p < 0.0001$], and Tukey’s post hoc analysis showed that CT β -positive signals were markedly reduced in 4- or 12-month-old 5XFAD mice than in age-matched WT mice. There was also an age-dependent reduction of CT β -positive signals in the dLGN [age: $F(1,177) = 14.69$, $p = 0.0002$], and Tukey’s post hoc test indicated that CT β -positive signals were considerably decreased in 12-month-old 5XFAD mice than in 4-month-old 5XFAD. There was no significant inter-

action between genotype and age in the dLGN [interaction: $F(1,177) = 0.5611, p = 0.4548$] (Figure 5C,F). The finding shows that the retinal projection to dLGN is more impaired by AD pathology than by aging.

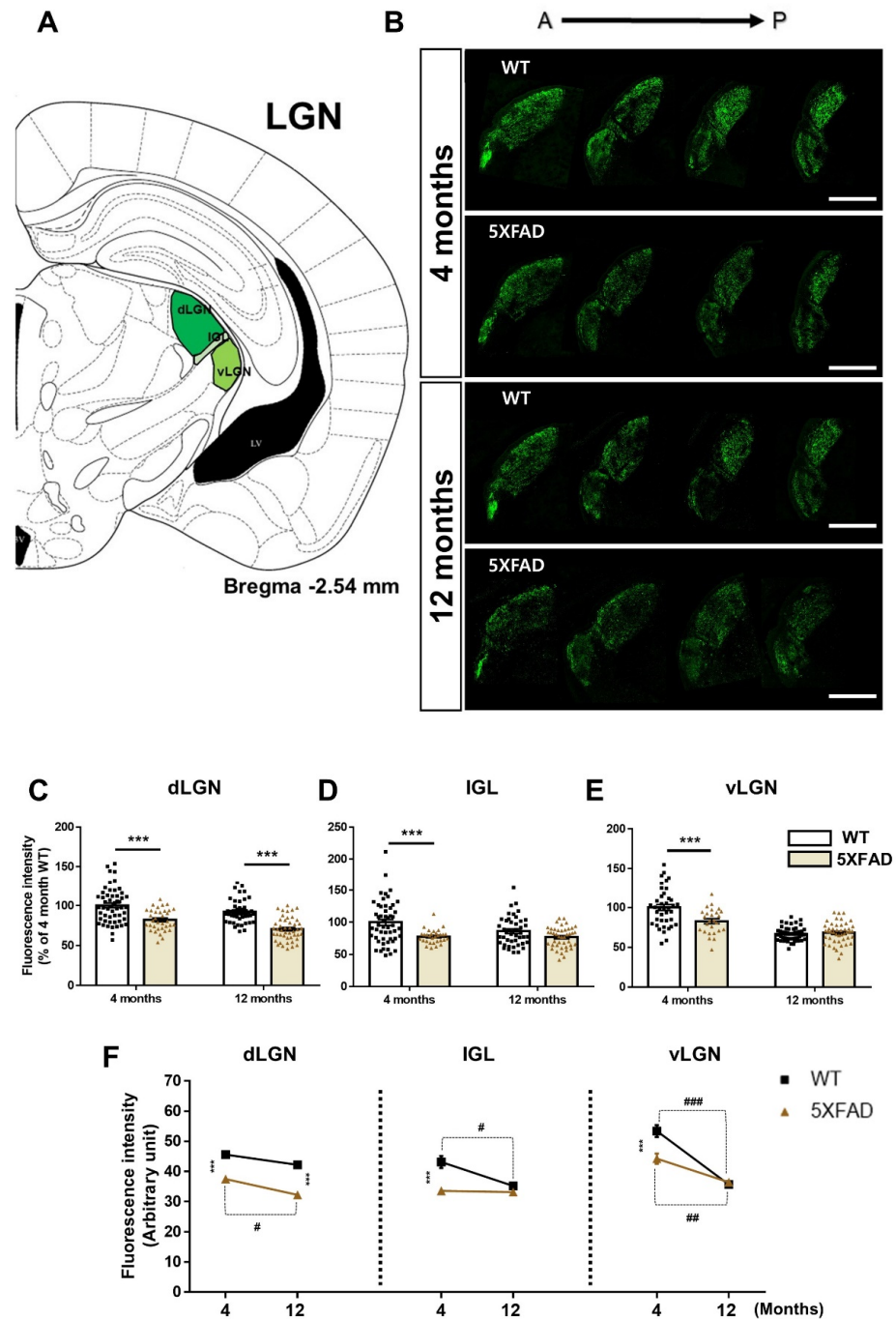


Figure 5. Changes of the retina-lateral geniculate nucleus (LGN) connections in WT and 5XFAD mice. (A) Image of a mouse brain atlas exhibiting the location of the LGN. (B) The representative images show CTβ transported from the retina to the LGN. Scale bar = 500 μm. The quantitative graphs exhibit the fluorescence intensity of CTβ (+) areas in the (C) dorsal lateral geniculate nucleus (dLGN), (D) intergeniculate leaflet (IGL), and the (E) ventral lateral geniculate nucleus (vLGN) of WT and 5XFAD mice (31–53 images of the brain sections were obtained from 5 mice in each group). (F) Comparison of the impairment of the retina-LGN pathways by aging and AD progression. Statistical analysis was conducted by two-way ANOVA, followed by Tukey’s post hoc test. *** $p < 0.001$, # $p < 0.05$, ## $p < 0.01$, and ### $p < 0.001$ indicate a significant difference.

Next, there was a significant difference in CT β fluorescence intensity values between the WT and 5XFAD groups in the IGL [genotype: $F(1,166) = 18.08, p < 0.0001$], and Tukey's post hoc analysis exhibited that CT β fluorescence intensity was strikingly reduced in 4-month-old 5XFAD mice than in 4-month-old WT mice. The fluorescence intensity of CT β decreased with age in the IGL [age: $F(1,166) = 3.965, p = 0.0481$], and Tukey's post hoc test displayed that CT β fluorescence intensity was significantly decreased in 12-month-old WT mice than in 4-month-old WT. There was no significant interaction between genotype and age in the IGL [interaction: $F(1,166) = 2.973, p = 0.0865$] (Figure 5D,F). Similar to the results of SCN, retinal to IGL projection was obviously impaired by AD pathology in 4-month-old 5XFAD mice. Additionally, impairments of this connection due to the normal aging process are prominent.

Finally, a significant difference in CT β -labeled signals was found in the vLGN of WT and 5XFAD groups [genotype: $F(1,160) = 9.364, p = 0.0026$], and Tukey's post hoc analysis showed that CT β -labeled signals were significantly reduced in 4-month-old 5XFAD mice compared to 4-month-old WT mice. The CT β -labeled signals decreased with age in the vLGN [age: $F(1,160) = 86.99, p < 0.0001$], and Tukey's post hoc test presented that CT β -labeled signals were significantly reduced in 12-month-old WT and 5XFAD mice than in 4-month-old WT and 5XFAD. There was significant interaction between genotype and age in the vLGN [interaction: $F(1,160) = 13.13, p = 0.0004$] (Figure 5E,F). The result reveals that retinal efferent projecting to the vLGN showed significance according to genotype in the early stage but showed significance according to genotype \times age interaction in the later stage. Taken together, our findings demonstrate that (1) the retinal efferents to the dLGN, IGL, vLGN are severely damaged before the prodromal stage of AD, (2) the retina-dLGN and vLGN pathways are consistently impaired between prodromal and severe stages, and (3) the retinal projections to the IGL and vLGN changed during normal aging.

3.5. Altered Retina-SC Connection in the A β -Overexpressing Mice

The SC is a region that relays visual information as part of the extrageniculate visual pathway from the retina to the higher visual cortex and plays an important role in visual function [40]. To reveal the retina-SC pathway, we conducted anterograde-tracing with CT β in 4- and 12-month-old WT and 5XFAD mice (Figure 6A,B). There was no impairment in the retina-SC pathway of 4-month-old 5XFAD mice compared to the 4-month-old WT mice. In contrast, the retina-SC connection of 12-month-old 5XFAD mice was significantly reduced compared to that of the 12-month-old WT mice [genotype: $F(1,112) = 77.66, p < 0.0001$]. Moreover, comparison of CT β -positive axon terminals between 4-month-old and 12-month-old mice showed a significant age-related decrease in the retina-SC projection of both WT and 5XFAD mice [age: $F(1,112) = 206, p < 0.0001$]. A two-way ANOVA displayed a significant interaction between genotype and age [interaction: $F(1,112) = 33.96, p < 0.0001$], and Tukey's post hoc analysis showed a more significant decrease in CT β -positive axon terminals in 12-month-old 5XFAD mice than in WT groups or 4-month-old 5XFAD mice (Figure 6C,D). Therefore, these anterograde-tracing results demonstrate that the retina-SC projection is severely impaired between the prodromal and severe stages of AD and is also damaged by the normal aging process.

3.6. Decreased Retina-MTN Projections in the Animal Model of AD

To reveal the changes in connectivity from the retina to the MTN in an AD mouse model, we detected the CT β -positive signals in MTN of 4- and 12-month-old WT and 5XFAD groups (Figure 7A,B). CT β -labeled signals were significantly reduced in 12 months of both WT and 5XFAD mice compared to 4 months [age: $F(1,73) = 115.4, p < 0.0001$] without a significant effect of genotype [genotype: $F(1,73) = 0.4698, p = 0.4953$] or a genotype \times age interaction [interaction: $F(1,73) = 2.369, p = 0.1281$] (Figure 7C,D). Thus, the fluorescence intensity of CT β in MTN changes only with age. These results suggest that retina-MTN pathways significantly degenerate during normal aging.

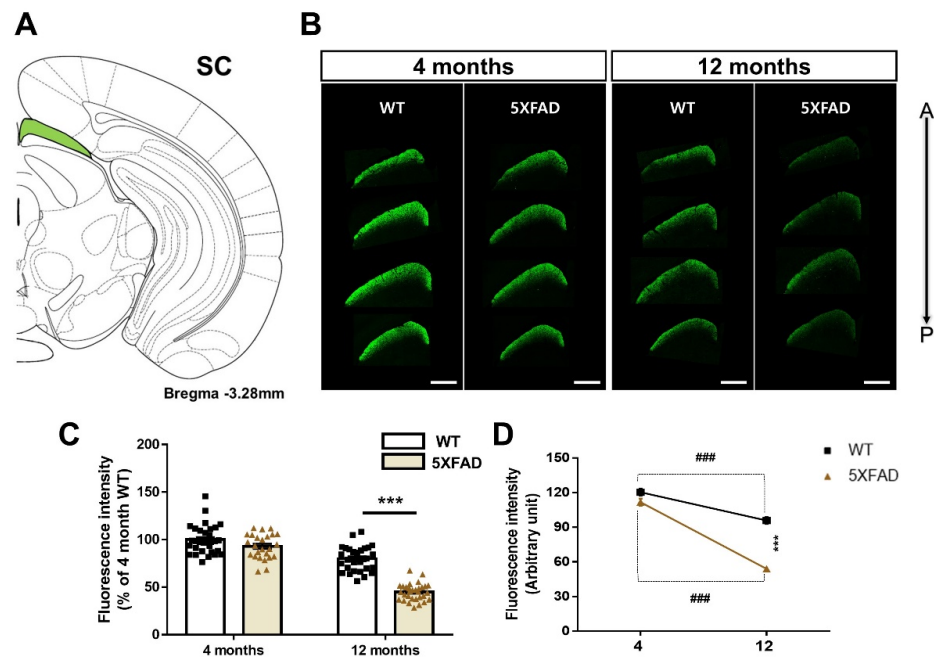


Figure 6. Degeneration of the retina-superior colliculus (SC) pathways in WT and 5XFAD mice. (A) Image of a mouse brain atlas illustrating the location of the SC. (B) The representative images indicate CTβ transported from the retina to the SC. Scale bar = 500 μm. (C) The quantitative graphs exhibit the fluorescence intensity of CTβ (+) areas in the SC of WT and 5XFAD mice (25–32 images of the brain sections were obtained from 5 mice in each group). (D) Comparison of the impairment of the retina-SC connection by aging and AD progression. Statistical analysis was conducted by two-way ANOVA, followed by Tukey’s post hoc test. *** $p < 0.001$ and ### $p < 0.001$ indicate a significant difference.

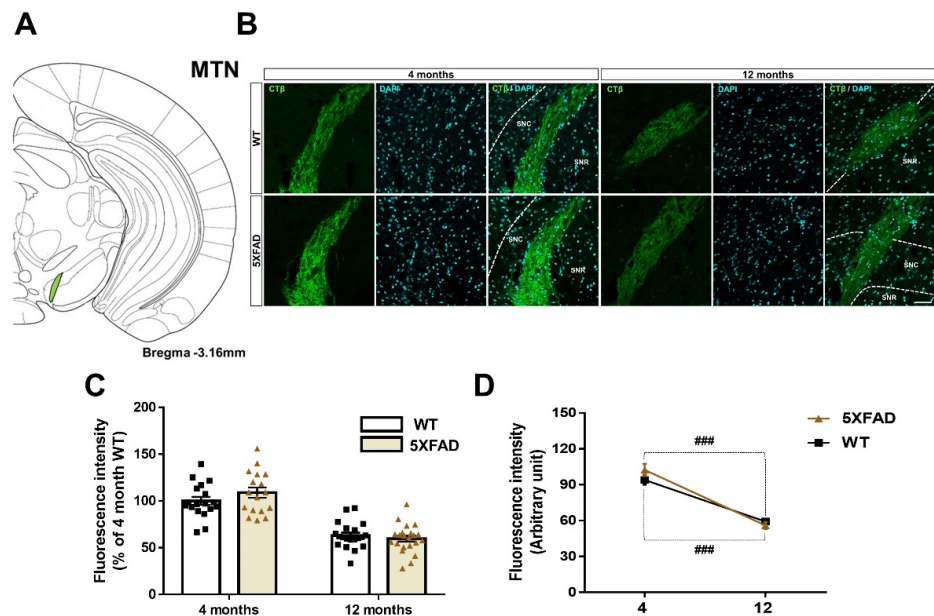


Figure 7. Neuroanatomic tract tracing of the retina-medial terminal nucleus of the accessory optic tract (MTN) projections in WT and 5XFAD mice. (A) Diagram of a mouse brain atlas illustrating the site of the MTN. (B) The representative images indicate CTβ transported from the retina to the MTN. Scale bar = 50 μm. (C) The quantitative graphs exhibit the fluorescence intensity of CTβ (+) areas in the MTN of WT and 5XFAD mice (18–22 images of the brain sections were obtained from 5 mice in each group). (D) Comparison of the impairment of the retina-MTN pathways by aging and AD progression. Statistical analysis was conducted by two-way ANOVA, followed by Tukey’s post hoc test. ### $p < 0.001$ indicate a significant difference.

3.7. Neurodegeneration in the Retinorecipient Area in the 5XFAD Mice

To investigate the cell death and synaptic degeneration in the exhibiting circuit damage from early AD stage, such as retina-SCN, retina-dLGN, retina-IGL, retina-vLGN, and retina-SC pathway, we conducted immunostaining to detect NeuN, a marker of neuronal nuclei (Figure 8A), and SYN, a marker of pre-synaptic terminals (Figure 9A). The 4-month-old 5XFAD mice indicated significant neuronal loss compared to WT mice in the dLGN, IGL, and vLGN (Figure 8B), which displayed robust accumulation of A β in 5XFAD mice. In 12-month-old 5XFAD mice, however, the SCN, dLGN, IGL, and vLGN regions exhibited significantly reduced numbers of NeuN-positive cells compared to WT mice; there was no significant reduce in the SC (Figure 8C). Interestingly, we found age- and AD progression-related neuronal loss in all regions (Figure 8D).

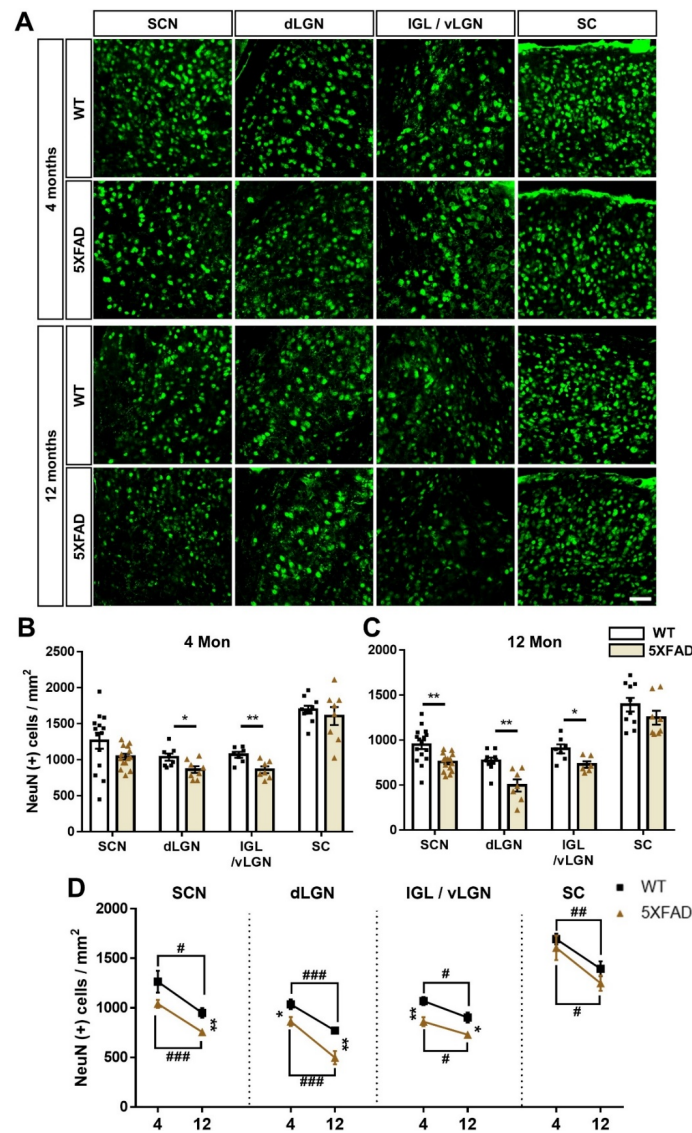


Figure 8. Neuronal loss in the retinorecipient area of the 5XFAD mice. (A) Representative images of neuronal nuclei (NeuN) in the SCN, dLGN, IGL, vLGN, and SC in the WT and 5XFAD mice. The scale bar is 50 μ m. (B,C) The quantitative graphs exhibit the NeuN (+) cells in the SCN, dLGN, IGL, vLGN, and SC of WT and 5XFAD mice (6–16 images of the brain sections were obtained from 5 mice in each group). Statistical analysis was conducted by a multiple *t*-test. (D) Comparison of the neuronal cell death by aging and AD progression. Statistical analysis was conducted by two-way ANOVA, followed by Tukey’s post hoc test. * $p < 0.05$, ** $p < 0.01$, # $p < 0.05$, ## $p < 0.01$, and ### $p < 0.001$ indicate a significant difference.

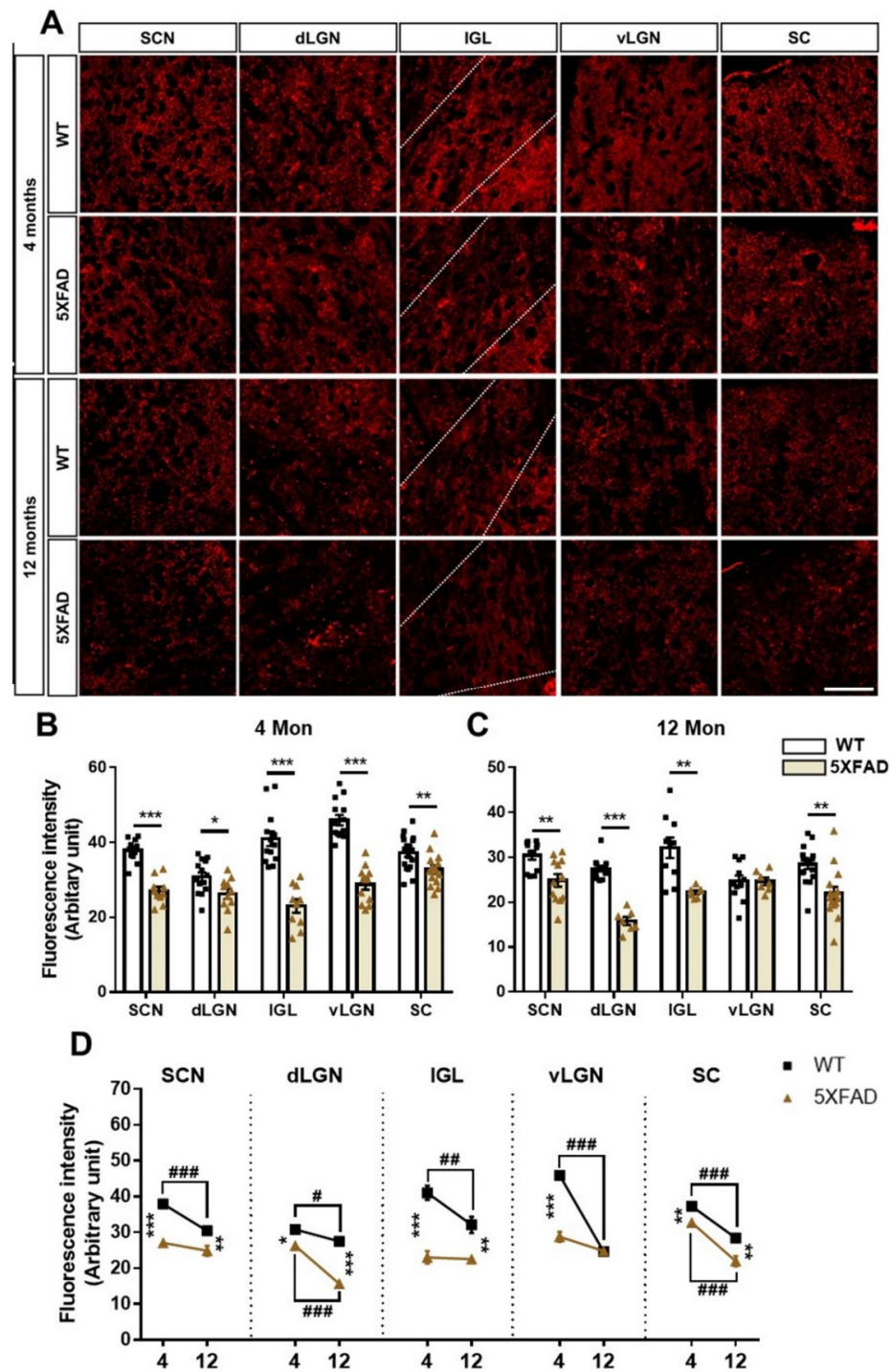


Figure 9. Synaptic degeneration in the retinorecipient area of the 5XFAD mice. (A) Representative images of pre-synaptic terminals in the SCN, dLGN, IGL, vLGN, and SC in the WT and 5XFAD mice. Pre-synaptic terminals were visualized using an anti-synaptophysin (SYN) antibody. The scale bar is 50 μ m. (B,C) The quantitative graphs exhibit the fluorescence intensity of SYN (+) areas in the SCN, dLGN, IGL, vLGN, and SC of WT and 5XFAD mice (7–18 images of the brain sections were obtained from 5 mice in each group). Statistical analysis was conducted by a multiple *t*-test. (D) Comparison of the synaptic loss by aging and AD progression. Statistical analysis was conducted by two-way ANOVA, followed by Tukey’s post hoc test. * $p < 0.05$, ** $p < 0.01$, *** $p < 0.001$, # $p < 0.05$, ## $p < 0.01$, and ### $p < 0.001$ indicate a significant difference.

The SYN fluorescence intensity was significantly decreased in the SCN, dLGN, IGL, vLGN, and SC in 4-month-old 5XFAD mice (Figure 9B). The SCN, dLGN, IGL, and SC showed significant pre-synaptic degeneration in 12-month-old 5XFAD mice compared to WT mice (Figure 9C). Notably, we observed age-related pre-synaptic loss in all regions (Figure 9D). In particular, the pre-synaptic loss occurring in the SCN, dLGN, IGL, vLGN, and SC could be closely related to the decrease in the CT β -positive signals in these regions. This finding could support a decrease in CT β -positive signals in the brain areas without A β deposits. These results reveal that the neuronal and synaptic losses occur with aging and AD progression and that the neurodegeneration could significantly affect the impairment of neural circuits in the brain with AD.

4. Discussion

Although visual circuit impairments in patients with AD patients has been reported at the macroscopic level [41], to the best of our knowledge, there is no study on the alteration of the visual circuit at the mesoscale level in the AD brain. Thus, our study aimed to provide direct anatomical evidence in a mouse model of AD by examining the topographical changes in various visual pathways between two different stages of AD. To investigate the visual circuitry of the AD brain, we intravitreally injected a non-transsynaptic anterograde trace CT β into the right eye of 4- and 12-month-old WT and 5XFAD mice. We demonstrated that the retinal projections to the SCN, dLGN, IGL, and vLGN were impaired in the 4-month-old 5XFAD mice, which exhibit no cognitive decline, compared to the age-matched WT. In addition, we found decreased connections of retina-dLGN and retina-SC in the 12-month-old 5XFAD mice, representing the severe stage of AD, compared to age-matched WT. Finally, we revealed that retinal connectivity decreases in several retinorecipient areas except for the OPN by normal aging. Furthermore, we found that neuronal loss and synaptic degeneration occur in retinorecipient regions with aging and AD progression and that this neurodegeneration could significantly affect the impairment of neural circuits. The present study demonstrated for the first time, the alteration of the visual pathways from the retina in the AD brain at the mesoscale level (Figure 10).

Retinal connections to the SCN, vLGN, and IGL were significantly impaired in the 4-month-old 5XFAD mice. However, these pathways did not show significant changes in CT β -positive signals between 4 and 12 months of 5XFAD (Figures 3D and 5F). One of the reasons is that these visual circuits in 5XFAD mice began to be impaired early, reaching thresholds already in 4-month-old 5XFAD mice. Neural circuit impairment that has reached a threshold result in early visual-related behavioral impairments. Many studies reported that the SCN, vLGN, and IGL are regions partially involved in circadian rhythms, such as the sleep-wake cycle [42,43]. Interestingly, circadian rhythm disturbance was observed in 4-month-old 5XFAD mice [23,44]. Thus, this evidence suggests that retinal projections to the SCN, vLGN, and IGL are already sufficiently impaired in 4-month-old 5XFAD mice, suggesting that alterations in these circuits may in part contribute to abnormal circadian rhythms.

Retinal projection to dLGN is consistently decreased in 4- and 12-month-old 5XFAD mice compared to WT of the same age (Figure 5F). These results demonstrate that the retina-dLGN pathway is continuously damaged during AD progression. Unfortunately, few studies have reported visual impairments, such as contrast sensitivity and color vision, in the 5XFAD mouse model. However, a study using an APP^{SWE}/PS1 ^{Δ E9} mouse model reported that contrast sensitivity and color vision were impaired in AD progression [45]. This finding indicates that the retina-dLGN pathway is persistently impaired in AD progression and damage to this circuitry can result in loss of contrast sensitivity and color vision.

The retina-SC pathway was dramatically reduced in the 12-month-old 5XFAD mice. However, this pathway did not significant changes in CT β -positive signals between 4 months of WT and 5XFAD mice (Figure 6D). The result suggests that damage to this pathway in 5XFAD mice begins at some point between 4 and 12 months of age. Some studies

show that the SC is involved in visuomotor functions, such as eye movement [46,47]. Visual acuity (optokinetic system) impairment was observed in 5XFAD mice from 6 months of age [22]. Thus, this evidence suggests that the connection between the retina and SC is significantly impaired between 4- and 12-month-old 5XFAD mice, suggesting that impairment of these circuits may in part contribute to visuomotor impairment.

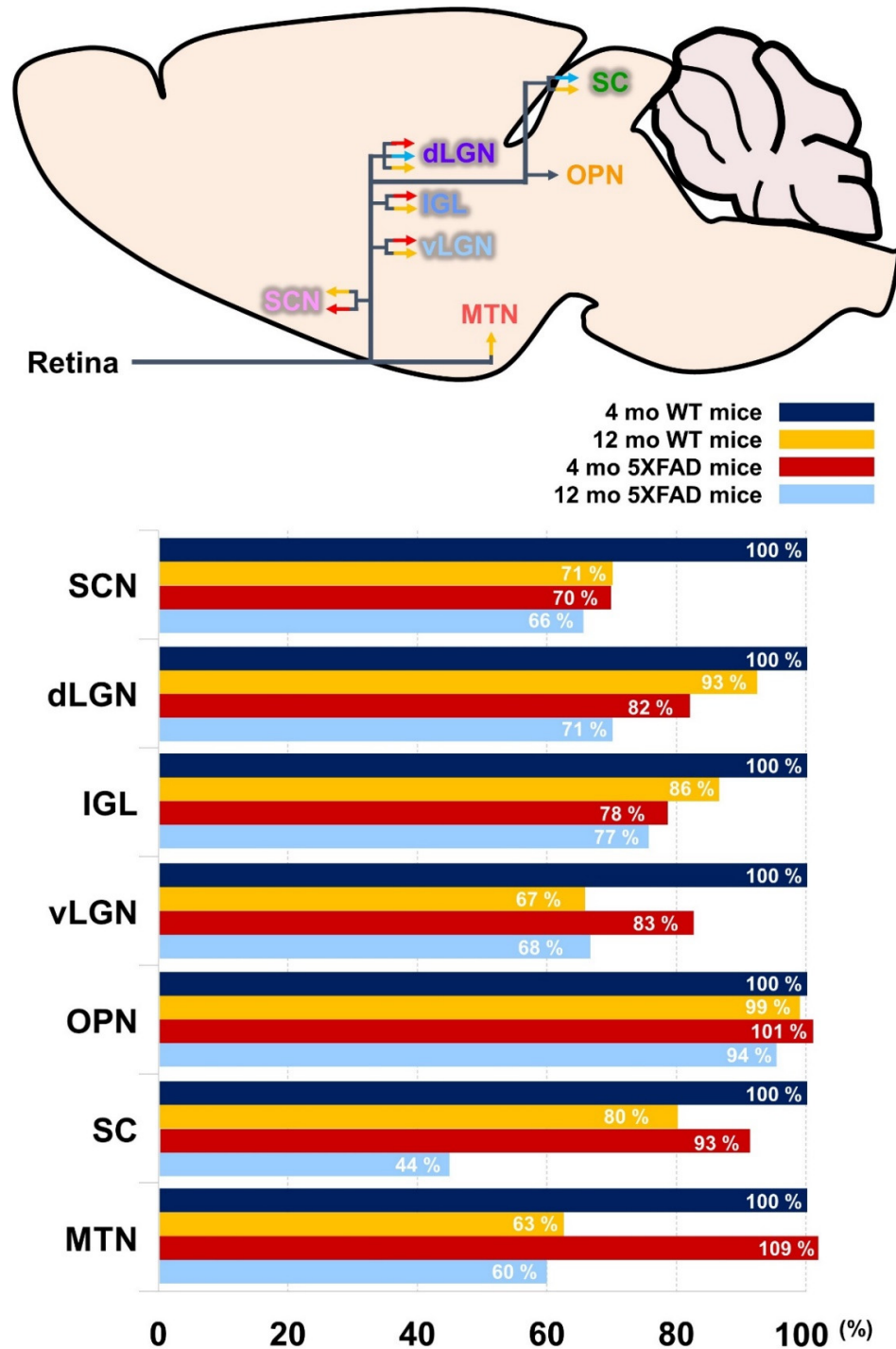


Figure 10. Schematic drawing and quantitative analysis of the altered visual pathways from the retina to the retinorecipient regions. The rate of degeneration of the visual pathways was normalized to those of 4-month-old WT mice indicated by the black bars. Red bars displayed regions that are impaired in early stage of AD. Blue bars indicate the damaged regions in late-stage of AD. Orange bars show regions damaged by aging.

It is well known that A β -induced neuronal dysfunctions induce neuronal circuit and network disturbances [48]. A key component of these neuronal dysfunctions is axonal degeneration. Axonal degeneration by A β toxicity preceded neuronal cell death. In contrast, inhibition of axonal degeneration through overexpression of nicotinamide mononucleotide adenylyltransferase 1 and Bcl-xl prevented neuronal cell death [49]. Therefore, A β observed in the retina (Figure 1E,F) can cause axonal degeneration of RGCs, resulting in disruption of the visual pathway. Similarly, the neuronal and synaptic loss occurred in the SCN, dLGN, IGL, vLGN, and SC of 4-month-old 5XFAD mice with/without A β deposition in those regions. These results could be due to already initiated neurodegeneration by intraneuronal A β -induced neurotoxicity, which appears much earlier than A β deposition [30,50].

It has been reported that 5XFAD mice, an A β overexpressing mouse model, exhibited similar levels of A β_{40} and A β_{42} peptides to those in the retina and neocortex of AD patients [51]. However, further experiments are needed to characterize the AD stage-dependent A β aggregates form in 5XFAD mouse retinas, as well as studies of retinal A β accumulation patterns in AD animal models and AD patients. Nevertheless, the 5XFAD mice showed stronger retinal and synaptic pathology than other AD mouse models [51]. Significantly increased A β concentrations were observed in the eyes of young 5XFAD mice without cognitive impairment compared to WT mice of the same age [18,52,53]. In addition, visual behavior abnormalities and circadian rhythm disturbance were reported in 5XFAD mice [18,22,23,44,54]. Although 5XFAD mouse models do not reflect all of the pathologies of AD and may not reflect the same visual pathway impairment as patients with AD, this model recapitulates several aspects, such as structural, molecular, cellular, and behavioral phenotypes, observed in AD patients. For instance, neuronal cell death and synaptic loss induced by A β are strong correlates of cognitive deficits in AD. Likewise, neurodegeneration induced by A β in 5XFAD mice is temporally associated with various dysfunctions. Therefore, since non-clinical studies are needed for developing treatment and diagnostic methods for AD, among various AD models, we chose 5XFAD mice, which accumulate the A β in the retina at the early stage and exhibit visual-related symptoms.

Our results suggested the retinal outputs were impaired in the 5XFAD mice. Unfortunately, most conventional tracers are unable to reveal the connectivity at the level of the cell-type-specific pathway [55]. Therefore, genetic tracing using cell-type-specific promoters should be used to investigate the disruption of glutamate-specific visual pathways. In addition, further studies on retinal projection damaged by hyperphosphorylated tau in tau animal models are needed, as phosphorylated tau may affect neural circuitry. Moreover, further studies using 5XFAD mice of various ages are needed to identify points where damage to the visual circuit is prominent. Nevertheless, the current research is the first to demonstrate the alteration in the visual pathways in an animal model of AD at the mesoscale level. Restoring damaged visual pathways with optogenetic stimulation, based on mesoscopic mapping of connectivity in the AD brain, could be a possible therapeutic approach for treating visual symptoms in patients with AD.

5. Conclusions

In this study, we examined the alteration of the visual pathway in the animal model of AD at the mesoscale level in both the early and late stages of AD. Taken together, the results of our study using 5XFAD mice demonstrated that (1) retinal projections to the SCN, dLGN, IGL, and vLGN were significantly impaired in the early stages of AD, (2) connections of the retina with dLGN and SC were disrupted in the late stages of AD, (3) the visual pathways in the brain with AD showed a trend towards accelerated degeneration during the AD progression, and (4) the visual circuits in the healthy brain degenerated according to aging.

Supplementary Materials: The following supporting information can be downloaded at: <https://www.mdpi.com/article/10.3390/cells11233901/s1>, Figure S1. Preparation of brain tissues of mice for CT β -positive signals and immunoreactivity analysis. Fixed mouse brains were coronally sectioned with a thickness of 30 μ m. From 1 to 2, the suprachiasmatic nucleus (SCN) is located from -0.22 mm to -0.82 mm of the bregma and is labeled in blue. From 3 to 4, the olivary pretectal nucleus (OPN) is located from -2.18 mm to -2.46 mm of the bregma and is labeled in violet. From 3 to 5, the lateral geniculate nucleus (LGN) is located from -2.18 mm to -2.92 mm of the bregma. The LGN subregions, the dorsal lateral geniculate nucleus (dLGN), intergeniculate leaflet (IGL), and ventral lateral geniculate nucleus (vLGN), are shown in yellow, orange, and green, respectively. From 6 to 7, the medial terminal nucleus of the accessory optic tract (MTN) is located from -3.16 mm to -3.28 mm of the bregma and is labeled in magenta. From 6 to 8, the superior colliculus (SC) is located from -3.16 mm to -4.36 mm of the bregma and is labeled in red. For quantification of CT β -positive signals, we obtained seven to eight sections per mouse in each region. For quantification of immunoreactivity, we acquired four sections per mouse in each region. The received images were subjected to topographical quantification and statistical analysis in a blind manner; Figure S2. The topographical schematic diagram for quantifying CT β -positive signals and immunoreactivity analysis in the brain tissues. (A) We show the process of the analysis steps for “area fraction (%)”, “fluorescence intensity (Arbitrary units)” and “(+) cells/mm²” using the ImageJ program. It displays the quantitative process of “Area fraction (%)” applied to histological analysis of 4G8-positive signals. (C) It shows the quantitative process of “Fluorescence intensity (Arbitrary units)” applied to histological analysis of CT β and SYN-positive signals. (D) It exhibits the quantitative process of “(+) cells/mm²” applied to histological analysis of NeuN (+) cells; Figure S3. Representative image of the photomicrograph validation of the intravitreal injection sites of the CT β in the retinal flat mount. Scale bar = 500 μ m; Figure S4. Representative images are immunohistochemical staining using anti-4G8 antibody in WT mice. Scale bar = 50 μ m; Figure S5. Validation of the application of the non-transsynaptic anterograde tracer CT β in the suprachiasmatic nucleus (SCN). (A) Representative images show the co-localization of CT β with synaptophysin (SYN), marker of presynaptic terminals. Scale bar = 10 μ m. (B) Profile analysis of representative images shows that CT β is predominantly co-localized with SYN. The graph shows the fluorescence intensity of the white dotted line. White arrows indicate where CT β (Green) and SYN (Red) coexist.

Author Contributions: Conceptualization, M.M. and H.-S.H.; methodology, Y.N., S.K. and J.K.; software, Y.N., S.K. and J.K.; validation, Y.N., S.K. and J.K.; formal analysis, Y.N. and S.K.; investigation, Y.N., S.K. and J.K.; resources, M.M. and H.-S.H.; data curation, Y.N., S.K. and J.K.; writing—original draft preparation, Y.N., S.K. and J.K.; writing—review and editing, M.M. and H.-S.H.; visualization, Y.N., S.K. and J.K.; supervision, M.M. and H.-S.H.; project administration, M.M. and H.-S.H.; funding acquisition, M.M., H.-S.H. and Y.N. All authors have read and agreed to the published version of the manuscript.

Funding: This research was funded by Basic Science Research Program of the National Research Foundation of Korea (NRF), which is funded by the Ministry of Science, ICT & Future Planning (NRF-2018R1D1A3B07041059 to M.M. and NRF-2022R1A6A3A13053190 to Y.N.) and was supported by a grant of the Korea Health Technology R&D Project through the Korea Health Industry Development Institute (KHIDI), funded by the Ministry of Health & Welfare, Republic of Korea (grant number: HF21C0021 to M.M.). This work was also supported by the Korea Brain Research Institute (KBRI) basic research program through KBRI funded by the Ministry of Science, ICT & Future Planning (grant number 22-BR-02-03 to H.-S.H.).

Institutional Review Board Statement: Not applicable.

Informed Consent Statement: Not applicable.

Data Availability Statement: Not applicable.

Acknowledgments: The authors thank all participants involved in this study.

Conflicts of Interest: The authors declare no conflict of interest.

References

1. Querfurth, H.W.; LaFerla, F.M. Alzheimer's disease. *N. Engl. J. Med.* **2010**, *362*, 329–344. [[CrossRef](#)] [[PubMed](#)]
2. Walsh, D.M.; Selkoe, D.J. A beta oligomers—A decade of discovery. *J. Neurochem.* **2007**, *101*, 1172–1184. [[CrossRef](#)] [[PubMed](#)]
3. Ripoli, C.; Cocco, S.; Li Puma, D.D.; Piacentini, R.; Mastrodonato, A.; Scala, F.; Puzzo, D.; D'Ascenzo, M.; Grassi, C. Intracellular accumulation of amyloid-beta (Abeta) protein plays a major role in Abeta-induced alterations of glutamatergic synaptic transmission and plasticity. *J. Neurosci.* **2014**, *34*, 12893–12903. [[CrossRef](#)]
4. Kim, S.; Nam, Y.; Jeong, Y.O.; Park, H.H.; Lee, S.K.; Shin, S.J.; Jung, H.; Kim, B.H.; Hong, S.B.; Park, Y.H.; et al. Topographical Visualization of the Reciprocal Projection between the Medial Septum and the Hippocampus in the 5XFAD Mouse Model of Alzheimer's Disease. *Int. J. Mol. Sci.* **2019**, *20*, 3992. [[CrossRef](#)]
5. Canter, R.G.; Penney, J.; Tsai, L.H. The road to restoring neural circuits for the treatment of Alzheimer's disease. *Nature* **2016**, *539*, 187–196. [[CrossRef](#)] [[PubMed](#)]
6. Jeon, S.G.; Kim, Y.J.; Kim, K.A.; Mook-Jung, I.; Moon, M. Visualization of Altered Hippocampal Connectivity in an Animal Model of Alzheimer's Disease. *Mol. Neurobiol.* **2018**, *55*, 7886–7899. [[CrossRef](#)] [[PubMed](#)]
7. Kim, S.; Nam, Y.; Kim, H.s.; Jung, H.; Jeon, S.G.; Hong, S.B.; Moon, M. Alteration of Neural Pathways and Its Implications in Alzheimer's Disease. *Biomedicines* **2022**, *10*, 845. [[PubMed](#)]
8. Wang, X.; Ren, P.; Mapstone, M.; Conwell, Y.; Porsteinsson, A.P.; Foxe, J.J.; Raizada, R.D.S.; Lin, F.; Alzheimer's Disease Neuroimaging Initiative. Identify a shared neural circuit linking multiple neuropsychiatric symptoms with Alzheimer's pathology. *Brain Imaging Behav.* **2019**, *13*, 53–64. [[CrossRef](#)] [[PubMed](#)]
9. Zott, B.; Busche, M.A.; Sperling, R.A.; Konnerth, A. What Happens with the Circuit in Alzheimer's Disease in Mice and Humans? *Annu. Rev. Neurosci.* **2018**, *41*, 277–297. [[CrossRef](#)]
10. Albers, M.W.; Gilmore, G.C.; Kaye, J.; Murphy, C.; Wingfield, A.; Bennett, D.A.; Boxer, A.L.; Buchman, A.S.; Cruickshanks, K.J.; Devanand, D.P.; et al. At the interface of sensory and motor dysfunctions and Alzheimer's disease. *Alzheimers Dement.* **2015**, *11*, 70–98. [[CrossRef](#)] [[PubMed](#)]
11. Lenoir, H.; Sieroff, E. Visual perceptual disorders in Alzheimer's disease. *Geriatr. Psychol. Neuropsychiatr. Vieil.* **2019**, *17*, 307–316. [[CrossRef](#)] [[PubMed](#)]
12. Ko, F.; Muthy, Z.A.; Gallacher, J.; Sudlow, C.; Rees, G.; Yang, Q.; Keane, P.A.; Petzold, A.; Khaw, P.T.; Reisman, C.; et al. Association of Retinal Nerve Fiber Layer Thinning with Current and Future Cognitive Decline: A Study Using Optical Coherence Tomography. *JAMA Neurol.* **2018**, *75*, 1198–1205. [[CrossRef](#)]
13. Paquet, C.; Boissonnot, M.; Roger, F.; Dighiero, P.; Gil, R.; Hugon, J. Abnormal retinal thickness in patients with mild cognitive impairment and Alzheimer's disease. *Neurosci. Lett.* **2007**, *420*, 97–99. [[CrossRef](#)] [[PubMed](#)]
14. Sadun, A.A.; Bassi, C.J. Optic nerve damage in Alzheimer's disease. *Ophthalmology* **1990**, *97*, 9–17. [[CrossRef](#)] [[PubMed](#)]
15. Lu, Y.; Li, Z.; Zhang, X.; Ming, B.; Jia, J.; Wang, R.; Ma, D. Retinal nerve fiber layer structure abnormalities in early Alzheimer's disease: Evidence in optical coherence tomography. *Neurosci. Lett.* **2010**, *480*, 69–72. [[CrossRef](#)]
16. Koronyo, Y.; Biggs, D.; Barron, E.; Boyer, D.S.; Pearlman, J.A.; Au, W.J.; Kile, S.J.; Blanco, A.; Fuchs, D.T.; Ashfaq, A.; et al. Retinal amyloid pathology and proof-of-concept imaging trial in Alzheimer's disease. *JCI Insight* **2017**, *2*, e93621. [[CrossRef](#)] [[PubMed](#)]
17. Chiassou, M.; Alarcon-Martinez, L.; Belforte, N.; Quintero, H.; Dotigny, F.; Destroismaisons, L.; Vande Velde, C.; Panayi, F.; Louis, C.; Di Polo, A. Tau accumulation in the retina promotes early neuronal dysfunction and precedes brain pathology in a mouse model of Alzheimer's disease. *Mol. Neurodegener.* **2017**, *12*, 58. [[CrossRef](#)] [[PubMed](#)]
18. Criscuolo, C.; Cerri, E.; Fabiani, C.; Capsoni, S.; Cattaneo, A.; Domenici, L. The retina as a window to early dysfunctions of Alzheimer's disease following studies with a 5xFAD mouse model. *Neurobiol. Aging* **2018**, *67*, 181–188. [[CrossRef](#)] [[PubMed](#)]
19. Martersteck, E.M.; Hirokawa, K.E.; Evarts, M.; Bernard, A.; Duan, X.; Li, Y.; Ng, L.; Oh, S.W.; Ouellette, B.; Royall, J.J.; et al. Diverse Central Projection Patterns of Retinal Ganglion Cells. *Cell Rep.* **2017**, *18*, 2058–2072. [[CrossRef](#)] [[PubMed](#)]
20. Wienbar, S.; Schwartz, G.W. The dynamic receptive fields of retinal ganglion cells. *Prog. Retin. Eye Res.* **2018**, *67*, 102–117. [[CrossRef](#)]
21. Monavarfeshani, A.; Sabbagh, U.; Fox, M.A. Not a one-trick pony: Diverse connectivity and functions of the rodent lateral geniculate complex. *Vis. Neurosci.* **2017**, *34*, E012. [[CrossRef](#)]
22. Zhang, M.; Zhong, L.; Han, X.; Xiong, G.; Xu, D.; Zhang, S.; Cheng, H.; Chiu, K.; Xu, Y. Brain and Retinal Abnormalities in the 5xFAD Mouse Model of Alzheimer's Disease at Early Stages. *Front. Neurosci.* **2021**, *15*, 681831. [[CrossRef](#)]
23. Sethi, M.; Joshi, S.S.; Webb, R.L.; Beckett, T.L.; Donohue, K.D.; Murphy, M.P.; O'Hara, B.F.; Duncan, M.J. Increased fragmentation of sleep-wake cycles in the 5XFAD mouse model of Alzheimer's disease. *Neuroscience* **2015**, *290*, 80–89. [[CrossRef](#)] [[PubMed](#)]
24. Giannoni, P.; Gaven, F.; de Bundel, D.; Baranger, K.; Marchetti-Gauthier, E.; Roman, F.S.; Valjent, E.; Marin, P.; Bockaert, J.; Rivera, S.; et al. Early administration of RS 67333, a specific 5-HT4 receptor agonist, prevents amyloidogenesis and behavioral deficits in the 5XFAD mouse model of Alzheimer's disease. *Front. Aging Neurosci.* **2013**, *5*, 96. [[CrossRef](#)] [[PubMed](#)]
25. Shvarts-Serebro, I.; Sheinin, A.; Gottfried, I.; Adler, L.; Schottlender, N.; Ashery, U.; Barak, B. miR-128 as a Regulator of Synaptic Properties in 5xFAD Mice Hippocampal Neurons. *J. Mol. Neurosci.* **2021**, *71*, 2593–2607. [[CrossRef](#)]
26. Lai, B.Q.; Qiu, X.C.; Zhang, K.; Zhang, R.Y.; Jin, H.; Li, G.; Shen, H.Y.; Wu, J.L.; Ling, E.A.; Zeng, Y.S. Cholera Toxin B Subunit Shows Transneuronal Tracing after Injection in an Injured Sciatic Nerve. *PLoS ONE* **2015**, *10*, e0144030. [[CrossRef](#)] [[PubMed](#)]

27. Angelucci, A.; Clasca, F.; Sur, M. Anterograde axonal tracing with the subunit B of cholera toxin: A highly sensitive immunohistochemical protocol for revealing fine axonal morphology in adult and neonatal brains. *J. Neurosci. Methods* **1996**, *65*, 101–112. [[CrossRef](#)] [[PubMed](#)]
28. Aviles-Trigueros, M.; Mayor-Torroglosa, S.; Garcia-Aviles, A.; Lafuente, M.P.; Rodriguez, M.E.; Miralles de Imperial, J.; Villegas-Perez, M.P.; Vidal-Sanz, M. Transient ischemia of the retina results in massive degeneration of the retinotectal projection: Long-term neuroprotection with brimonidine. *Exp. Neurol.* **2003**, *184*, 767–777. [[CrossRef](#)]
29. Kimura, R.; Ohno, M. Impairments in remote memory stabilization precede hippocampal synaptic and cognitive failures in 5XFAD Alzheimer mouse model. *Neurobiol. Dis.* **2009**, *33*, 229–235. [[CrossRef](#)]
30. Eimer, W.A.; Vassar, R. Neuron loss in the 5XFAD mouse model of Alzheimer’s disease correlates with intraneuronal Abeta42 accumulation and Caspase-3 activation. *Mol. Neurodegener.* **2013**, *8*, 2. [[CrossRef](#)]
31. Nam, Y.; Shin, S.J.; Park, Y.H.; Kim, M.J.; Jeon, S.G.; Lee, H.; Choi, Y.; Kim, T.J.; Shin, S.M.; Kim, J.J.; et al. Platycodon grandiflorum Root Protects against Abeta-Induced Cognitive Dysfunction and Pathology in Female Models of Alzheimer’s Disease. *Antioxidants* **2021**, *10*, 207. [[CrossRef](#)] [[PubMed](#)]
32. Grant, R.A.; Wong, A.A.; Fertan, E.; Brown, R.E. Whisker exploration behaviours in the 5x FAD mouse are affected by sex and retinal degeneration. *Genes Brain Behav.* **2020**, *19*, e12532. [[CrossRef](#)]
33. Chang, B.; Hawes, N.L.; Hurd, R.E.; Davisson, M.T.; Nusinowitz, S.; Heckenlively, J.R. Retinal degeneration mutants in the mouse. *Vision Res.* **2002**, *42*, 517–525. [[CrossRef](#)] [[PubMed](#)]
34. Levkovitch-Verbin, H. Animal models of optic nerve diseases. *Eye* **2004**, *18*, 1066–1074. [[CrossRef](#)] [[PubMed](#)]
35. Jain, N.S.; Jain, S.V.; Wang, X.; Neely, A.J.; Tahtali, M.; Jain, S.; Lueck, C.J. Visualization of Nerve Fiber Orientations in the Human Optic Chiasm Using Photomicrographic Image Analysis. *Investig. Ophthalmol. Vis. Sci.* **2015**, *56*, 6734–6739. [[CrossRef](#)] [[PubMed](#)]
36. Park, S.W.; Kim, J.H.; Park, S.M.; Moon, M.; Lee, K.H.; Park, K.H.; Park, W.J.; Kim, J.H. RAGE mediated intracellular Abeta uptake contributes to the breakdown of tight junction in retinal pigment epithelium. *Oncotarget* **2015**, *6*, 35263–35273. [[CrossRef](#)]
37. Park, S.W.; Kim, J.H.; Mook-Jung, I.; Kim, K.W.; Park, W.J.; Park, K.H.; Kim, J.H. Intracellular amyloid beta alters the tight junction of retinal pigment epithelium in 5XFAD mice. *Neurobiol. Aging* **2014**, *35*, 2013–2020. [[CrossRef](#)]
38. Welsh, D.K.; Takahashi, J.S.; Kay, S.A. Suprachiasmatic nucleus: Cell autonomy and network properties. *Annu. Rev. Physiol.* **2010**, *72*, 551–577. [[CrossRef](#)]
39. Derrington, A. The lateral geniculate nucleus. *Curr. Biol.* **2001**, *11*, R635–R637. [[CrossRef](#)] [[PubMed](#)]
40. Tohmi, M.; Meguro, R.; Tsukano, H.; Hishida, R.; Shibuki, K. The extrageniculate visual pathway generates distinct response properties in the higher visual areas of mice. *Curr. Biol.* **2014**, *24*, 587–597. [[CrossRef](#)]
41. Nishioka, C.; Poh, C.; Sun, S.W. Diffusion tensor imaging reveals visual pathway damage in patients with mild cognitive impairment and Alzheimer’s disease. *J. Alzheimers Dis.* **2015**, *45*, 97–107. [[CrossRef](#)]
42. Hastings, M.H.; Maywood, E.S.; Brancaccio, M. Generation of circadian rhythms in the suprachiasmatic nucleus. *Nat. Rev. Neurosci.* **2018**, *19*, 453–469. [[CrossRef](#)] [[PubMed](#)]
43. Lewandowski, M.H.; Usarek, A. Effects of intergeniculate leaflet lesions on circadian rhythms in the mouse. *Behav. Brain Res.* **2002**, *128*, 13–17. [[CrossRef](#)] [[PubMed](#)]
44. Song, H.; Moon, M.; Choe, H.K.; Han, D.H.; Jang, C.; Kim, A.; Cho, S.; Kim, K.; Mook-Jung, I. Abeta-induced degradation of BMAL1 and CBP leads to circadian rhythm disruption in Alzheimer’s disease. *Mol. Neurodegener.* **2015**, *10*, 13. [[CrossRef](#)] [[PubMed](#)]
45. Vit, J.P.; Fuchs, D.T.; Angel, A.; Levy, A.; Lamensdorf, I.; Black, K.L.; Koronyo, Y.; Koronyo-Hamaoui, M. Color and contrast vision in mouse models of aging and Alzheimer’s disease using a novel visual-stimuli four-arm maze. *Sci. Rep.* **2021**, *11*, 1255. [[CrossRef](#)] [[PubMed](#)]
46. Ahmadlou, M.; Zweifel, L.S.; Heimel, J.A. Functional modulation of primary visual cortex by the superior colliculus in the mouse. *Nat. Commun.* **2018**, *9*, 3895. [[CrossRef](#)]
47. Wurtz, R.H.; Albano, J.E. Visual-motor function of the primate superior colliculus. *Annu. Rev. Neurosci.* **1980**, *3*, 189–226. [[CrossRef](#)] [[PubMed](#)]
48. Palop, J.J.; Mucke, L. Amyloid-beta-induced neuronal dysfunction in Alzheimer’s disease: From synapses toward neural networks. *Nat. Neurosci.* **2010**, *13*, 812–818. [[CrossRef](#)]
49. Alobuia, W.M.; Xia, W.; Vohra, B.P. Axon degeneration is key component of neuronal death in amyloid-beta toxicity. *Neurochem. Int.* **2013**, *63*, 782–789. [[CrossRef](#)]
50. Oakley, H.; Cole, S.L.; Logan, S.; Maus, E.; Shao, P.; Craft, J.; Guillozet-Bongaarts, A.; Ohno, M.; Disterhoft, J.; Van Eldik, L.; et al. Intraneuronal beta-amyloid aggregates, neurodegeneration, and neuron loss in transgenic mice with five familial Alzheimer’s disease mutations: Potential factors in amyloid plaque formation. *J. Neurosci.* **2006**, *26*, 10129–10140. [[CrossRef](#)] [[PubMed](#)]
51. Alexandrov, P.N.; Pogue, A.; Bhattacharjee, S.; Lukiw, W.J. Retinal amyloid peptides and complement factor H in transgenic models of Alzheimer’s disease. *Neuroreport* **2011**, *22*, 623–627. [[CrossRef](#)] [[PubMed](#)]
52. Parthasarathy, R.; Chow, K.M.; Derafshi, Z.; Fautsch, M.P.; Hetling, J.R.; Rodgers, D.W.; Hersh, L.B.; Pepperberg, D.R. Reduction of amyloid-beta levels in mouse eye tissues by intra-vitreally delivered neprilysin. *Exp. Eye Res.* **2015**, *138*, 134–144. [[CrossRef](#)] [[PubMed](#)]
53. Pogue, A.I.; Dua, P.; Hill, J.M.; Lukiw, W.J. Progressive inflammatory pathology in the retina of aluminum-fed 5x FAD transgenic mice. *J. Inorg. Biochem.* **2015**, *152*, 206–209. [[CrossRef](#)] [[PubMed](#)]

-
54. Adaikkan, C.; Wang, J.; Abdelaal, K.; Middleton, S.J.; Bozzelli, P.L.; Wickersham, I.R.; McHugh, T.J.; Tsai, L.H. Alterations in a cross-hemispheric circuit associates with novelty discrimination deficits in mouse models of neurodegeneration. *Neuron* **2022**, *110*, 3091–3105. [[CrossRef](#)]
 55. Xu, X.; Holmes, T.C.; Luo, M.H.; Beier, K.T.; Horwitz, G.D.; Zhao, F.; Zeng, W.; Hui, M.; Semler, B.L.; Sandri-Goldin, R.M. Viral Vectors for Neural Circuit Mapping and Recent Advances in Trans-synaptic Anterograde Tracers. *Neuron* **2020**, *107*, 1029–1047. [[CrossRef](#)]